**Atmospheric
Chemistry
and Physics
Discussions**

Factor analysis of combined organic and inorganic aerosol mass spectra from high resolution aerosol mass spectrometer measurements

Y. L. Sun[1], Q. Zhang[2], J. J. Schwab[3], T. Yang[1], N. L. Ng[4], and K. L. Demerjian[3]

[1]State Key Laboratory of Atmospheric Boundary Layer Physics and Atmospheric Chemistry, Institute of Atmospheric Physics, Chinese Academy of Sciences, Beijing, China
[2]Department of Environmental Toxicology, University of California, Davis, California, USA
[3]Atmospheric Sciences Research Center, State University of New York at Albany, Albany, New York, USA
[4]School of Chemical and Biomolecular Engineering and School of Earth and Atmospheric Sciences, Georgia Institute of Technology, Atlanta, Georgia, USA

Title Page

Abstract	Introduction
Conclusions	References
Tables	Figures

|◄ | ►|
◄ | ►

Back | Close

Full Screen / Esc

Printer-friendly Version

Interactive Discussion

Abstract

The high resolution mass spectra of organic and inorganic aerosols from aerosol mass spectrometer (AMS) measurements were first combined into positive matrix factorization (PMF) analysis to investigate the sources and evolution processes of atmospheric
5   aerosols. The new approach is able to study the mixing of organic aerosols (OA) and inorganic species, the acidity of OA factors, and the fragment ion patterns related to photochemical processing. In this study, PMF analysis of the unified AMS spectral matrices resolved 8 factors for the submicron aerosols measured at Queens College in New York City in summer 2009. The hydrocarbon-like OA (HOA) and cooking OA (COA) contain
10   very minor inorganic species, indicating the different sources and mixing characteristics between primary OA and secondary species. The two factors that are primarily ammonium sulfate (SO_4-OA) and ammonium nitrate (NO_3-OA), respectively, are overall neutralized, of which the OA in SO_4-OA shows the highest oxidation state (O/C = 0.69) among OA factors. The semi-volatile oxygenated OA comprises two components, i.e.,
15   a less oxidized (LO-OOA) and a more oxidized (MO-OOA). The MO-OOA represents a local photochemical product with the diurnal profile exhibiting a pronounced noon peak, consistent with those of formaldehyde (HCHO) and $O_x (= O_3 + NO_2)$. The much higher NO^+/NO_2^+ fragment ion ratio in MO-OOA than that from ammonium nitrate alone provides evidence for the formation of organic nitrates. The amine-related nitrogen-
20   enriched OA (NOA) contains $\sim 25\%$ of acidic inorganic salts, elucidating the formation of secondary OA from amines in acidic environments. The size distributions derived from 3-dimensional size-resolved mass spectra show distinct diurnal evolving behaviors for different OA factors, but overall a progressing evolution from smaller to larger particle mode as a function of oxidation states. Our results demonstrate that PMF anal-
25   ysis by incorporating inorganic aerosols is of importance for gaining more insights into the sources and processes, mixing characteristics, and acidity of OA.

1 Introduction

Atmospheric fine particles exert a serious impact on air quality and visibility reduction (Watson, 2002), and harmful effects on human health (Pope III et al., 2002, 2009). Organic aerosols (OA) – a major fraction of fine particles (Zhang et al., 2007a; Jimenez

5 et al., 2009) have a highly uncertain impacts on radiative forcing (Forster et al., 2007). Current models often underestimate the OA substantially, mainly due to the unknown sources, sinks, and formation mechanisms (e.g., aqueous-phase production of secondary OA) (Heald et al., 2005; Volkamer et al., 2006; Dzepina et al., 2009; Wood et al., 2010; Heald et al., 2011). Thus, a better understanding of the sources and evo-

10 lution processes of OA is of importance for assessing aerosol impacts and reducing the uncertainties in models.

OA from a wide variety of source emissions are either primary from direct emissions, e.g., combustion of fossil fuels and biomass burning, or secondary which is formed via gas-to-particle conversions such as oxidation of volatile organic compounds (VOCs)

15 and/or aqueous-phase production. The atmospheric evolution such as aging, mixing, and cloud processing further leads to a change of the chemical, physical and optical properties of both primary OA (POA) and secondary OA (SOA). While the primary emissions of OA are fairly well understood, there are considerable uncertainties in quantification and characterization of SOA. The traditional EC-tracer method (Turpin

20 and Huntzicker, 1995) may involve large uncertainties in quantification of secondary organic carbon (SOC) due to either the differences in defining OC and EC from thermal-optical analysis (Khan et al., 2011) or various $OC/EC_{primary}$ ratio from different combustion emission sources. The molecular-marker based chemical mass balance (CMB) receptor model is capable of quantifying the contributions of primary sources, but of-

25 ten a large fraction of secondary species remains uncharacterized (Schauer and Cass, 2000; Zheng et al., 2002). In addition, the techniques above often rely on the measurements over hours to days, which is difficult to capture the fast evolution processes of OA in the atmosphere.

Title Page

Abstract | Introduction

Conclusions | References

Tables | Figures

|◄ | ►|

◄ | ►

Back | Close

Full Screen / Esc

Printer-friendly Version

Interactive Discussion

The Aerodyne Aerosol Mass Spectrometers (AMS) using thermal vaporization (typically 600 °C) and electron impact ionization ($\sim 70\,eV$) allow us to obtain the ensemble mass spectra of OA in real time, typically in a few seconds to minutes (Jayne et al., 2000; Drewnick et al., 2005; DeCarlo et al., 2006). The custom principle component analysis (CPCA) was firstly used to deconvolve the OA into different factors that are associated with different sources and processes (Zhang et al., 2005a). The hydrocarbon-like OA (HOA), a surrogate of POA from traffic emissions, and oxygenated OA (OOA), a surrogate of SOA, were ubiquitously resolved at urban locations. HOA often shows tight correlations with the tracers for primary emissions, e.g., NO_x, BC, and CO, etc., while OOA is generally correlated with secondary inorganic species, e.g., sulfate and/or nitrate (Zhang et al., 2005b). The multiple component analysis (MCA) was further developed to characterize the potential sub-OOA factors, e.g., highly oxidized OOA (OOA-I) and less oxidized OOA (OOA-II) (Zhang et al., 2007a). MCA analysis of 37 AMS datasets in the Northern Hemisphere shows an overall dominance of OOA at various atmospheric environments from urban, urban downwind, to rural and remote sites (Zhang et al., 2007a). The positive matrix factorization (PMF) (Paatero and Tapper, 1994), a bilinear model that constrains the factors to be non-negative and physically meaningful, is currently mostly used for OA mass spectra analysis (Lanz et al., 2007; Ulbrich et al., 2009; Zhang et al., 2011). Various POA components like HOA, cooking OA (COA), and biomass burning OA (BBOA), and SOA components like semi-volatile OOA (SV-OOA) and low-volatility OOA (LV-OOA) are broadly identified depending on sites, seasons, and sources emissions. The OA factors together with the measurements of hygroscopicity, volatility, and oxidation states significantly improve our understanding on the sources and evolution processes of OA in the atmosphere (Jimenez et al., 2009).

The recent PMF analysis of high resolution mass spectra (HRMS) further improves the differentiation of OA factors and also allows determining the oxidation state of each factor (Aiken et al., 2009; DeCarlo et al., 2010; Sun et al., 2011c). Given that the atmospheric evolution of OA might involve a progressive oxidation from fresh to highly

aged OA associated with a change of functionalities, volatilities, and oxidative prop-
erties (Heald et al., 2010; Ng et al., 2010; Sun et al., 2011b), more sub-OOA fac-
tors are expected, but difficult to be resolved due to a lack of collocated variables.
Slowik et al. (2010b) firstly combined the OA spectra from AMS measurements with
5 the VOCs measured by a proton transfer reaction-mass spectrometer (PTR-MS). PMF
analysis of the unified dataset shows the capability in resolving more OOA factors and
improving the interpretations of their sources and photochemical processes. Docherty
et al. (2011) performed the PMF analysis to the combined ambient and thermally de-
nuded OA spectra (TD-PMF-AMS) during the 2005 Study of Organic Aerosols at River-
10 side (SOAR-1). The TD-PMF-AMS with improved differentiation of OA factors identified
two more secondary OOA factors in addition to the previous SV-OOA and LV-OOA. De-
spite this, the two approaches above are often limited by the collocated measurements
of VOCs by PTR-MS or thermally denuded OA spectra that are not available in field
studies. Furthermore, previous PMF analysis is only performed to AMS OA spectra,
15 while the inorganic species, e.g., sulfate and nitrate are used as external tracers for
comparison purpose. Since the organic and inorganic species from different sources
and formation mechanisms are often externally or internally mixed as a function of
aerosol evolution in the atmosphere, PMF analysis of OA spectra only may bury the
intrinsic relationship between organic and inorganic species.

20 In this study, we re-analyzed the 3-week HRMS of organic and inorganic aerosols
(IOA) measured by an Aerodyne High Resolution Time-of-Flight AMS (HR-AMS, De-
Carlo et al., 2006) at Queens College (QC) in New York City (NYC) in summer, 2009
(Sun et al., 2011c). For the first time, we integrate the organic and inorganic spectral
matrices into one unified dataset for PMF analysis. The sources, mixing characteris-
25 tics, acidity, and photochemical processing of OA and IOA are investigated. In addition,
the size distributions of OA factors are derived from 3-dimensional size-resolved mass
spectra, and their implications in studying the sources and processes of OA are dis-
cussed.

2 Method

2.1 AMS measurements and data analyses

The HR-AMS was deployed on the campus of Queens College (40.74° N, 73.82° W) in NYC from 13 July through 3 August 2009 for in-situ measurements of the mass concentrations, chemical composition and size distributions of non-refractory submicron aerosol (NR-PM$_1$) species The descriptions of the sampling site and operations of the HR-AMS and collocated instruments have been detailed in Sun et al. (2011c) and Lin et al. (2012) The HR-AMS data were reanalyzed with the latest versions of standard AMS software (http://cires.colorado.edu/jimenez-group/ToFAMSResources/ ToFSoftware/index.html). The mass concentrations and size distributions of NR-PM$_1$ species, and the elemental composition of OA were obtained. In addition, the high resolution (HR) mass spectral matrices and 3-dimensional size-resolved mass spectra were extracted for the subsequent PMF analysis and size deconvolution, respectively. All data in this study is reported at Eastern Standard Time (EST = local time −1 h).

2.2 Preparation of mass spectral and error matrices

The procedures for preparation of HR mass spectral and error matrices for PMF analysis have been described in DeCarlo et al. (2010). Following the same procedures, the mass spectral and error matrices of inorganic species including sulfate, nitrate, ammonium, and chloride were prepared and integrated with those of OA into one unified dataset. Only major fragment ions for each inorganic species are included. They are SO^+ (*m/z* 48), SO_2^+ (*m/z* 64), SO_3^+ (*m/z* 80), HSO_3^+ (*m/z* 81), and $H_2SO_4^+$ (*m/z* 98) for sulfate, NO^+ (*m/z* 30) and NO_2^+ (*m/z* 46) for nitrate, NH^+ (*m/z* 15), NH_2^+ (*m/z* 16), NH_3^+ (*m/z* 17) for ammonium, and Cl^+ (*m/z* 35) and HCl^+ (*m/z* 36) for chloride. Ions that are constrained, i.e., scaled to ion intensities (e.g., according to the known isotope ratios for isotopic ions), are not included. The sum of selected fragment ions represents a major fraction of nitrate (96.2 %), ammonium (99.6 %) and chloride (75.8 %), and ~ half of

13304

sulfate (50.6 %), respectively. Further, these fragment ions show very tight correlations with the total mass concentration of each species ($r^2 \approx 1$, Fig S1 in supplement), indicating that the selected ions are well representative of each inorganic species. The concentrations of inorganic species in each factor after PMF analysis are derived from the sum of fragment ions divided by their fractional contributions in the corresponding species (Fig. S1).

2.3 Positive matrix factorization (PMF)

As a standard multivariate factor analysis approach, the PMF (Paatero and Tapper, 1994) uses the positively constrained bilinear model to deconvolve the HR mass spectral matrix (x_{ij}; dimensions: $m \times n$) into distinct factors (p) without a priori assumptions for either time series or mass spectral profiles.

$$x_{ij} = \sum_p g_{ip} f_{pj} + e_{ij} \qquad (1)$$

where i and j refer to row and column indices in the matrix, respectively, and p is the number of factors in the solution. x_{ij} is the measured concentrations of ion fragment j at time-step i. g_{ip} is the concentration of a given factor p at time-step i, and f_{pj} is the fraction of an ion fragment j in the mass spectral profile of factor p, and e_{ij} is the residual not fit by the model. PMF solves the Eq. (1) by minimizing the sum of the error weighed squared residuals ("Q").

$$Q = \sum_{i=1}^{m} \sum_{j=1}^{n} (e_{ij}/\sigma_{ij})^2 \qquad (2)$$

where σ_{ij} is the estimated error of ion fragment j at time-step i in the $m \times n$ matrix. The solutions are constrained to be positive which is physically meaningful in real atmospheric environment. The PMF analysis using PMF2 algorithm (v 4.2) in robust mode was performed to the combined HR matrices of OA and IOA. The PMF2 solutions were

Factor analysis of combined organic and inorganic aerosol spectra

Y. L. Sun et al.

then evaluated with an Igor Pro-based PMF Evaluation Tool (PET, v2.04) (Ulbrich et al., 2009) following the procedures detailed in Zhang et al. (2011) (Fig. S2). The PMF analysis was also performed to the HR matrices of OA, and the results of 5-factor solution were presented in Sun et al. (2011c).

5   After a detailed evaluation of mass spectral profiles, time series, diurnal variations, and correlations with external tracers, the 8-factor solution with fPeak = 0 (Q/Q_{exp} = 1.5) was chosen. The mass spectral profiles and diurnal variations of 7-factor and 9-factor solutions are shown in Figs. S3 and S4, respectively. The eight factors identified include two primary factors, i.e., a hydrocarbon-like OA (HOA, O/C = 0.04) and

10   a cooking OA (COA, O/C = 0.13), two semi-volatile oxygenated OA (OOA) factors, i.e., a more oxidized (MO-OOA, O/C = 0.48) and a less oxidized (LO-OOA, O/C = 0.27), a low volatility OOA (LV-OOA, O/C = 0.59), a nitrogen-enriched OA (NOA, O/C = 0.28), and two factors that are primarily ammonium sulfate (SO$_4$-OA, O/C = 0.69) and ammonium nitrate (NO$_3$-OA, O/C = 0.14), respectively. The primary HOA and COA show very

15   similar spectral patterns and time series to those reported in Sun et al. (2011c) (Figs. 1 and S5). This suggests that PMF analysis of the combined HR matrices has minor effects on primary factors, consistent with the different sources of POA from secondary species. However, the new approach appear to split the previous SV-OOA and LV-OOA in Sun et al. (2011c) into LO-OOA and MO-OOA, and LV-OOA and SO$_4$-OA, respec-

20   tively, in this study. Indeed, the combined mass spectra and time series of LO-OOA and MO-OOA, and LV-OOA and SO$_4$-OA are very similar to those of SV-OOA and LV-OOA, respectively, in Sun et al. (2011c) (Fig. 1c, d and Fig. S5c, d). Due to the absence of collocated measurement of HCHO in Sun et al. (2011c), the PMF resolution was limited to 5-factors. Here, the OA mass spectra were re-analyzed with PMF, and the

25   resolution were extended to 6-factor, i.e., HOA, COA, NOA, LO-OOA, MO-OOA, and LV-OOA. The results of 6-factor solution are then compared with 8-factor solution from PMF analysis of the combined spectra in Fig. S6. Again, the POA factors of HOA and COA from the two different approaches show much similarity in both spectral profiles and time series. While the spectral patterns are overall similar, the OOA factors show

some differences in time series, mainly due to the apportionment of part OOA into SO$_4$-OA factor.

2.4 Determination of the size distributions of OA factors

The size distributions of OA factors are of importance for investigation of their properties, hygroscopicity, and evolution processes. Recently, a 3-dimensional (3-D; dimensions: date/time, size, and *m/z*) factorization models was developed to derive the size distribution of OA factors (Ulbrich et al., 2012). In this study, we apply the multiple linear regression technique (Eq. 3) to the 3-D size-resolved mass spectra for determination of the size distributions of OA assuming that (1) the mass spectrum is a linear combination of six OA factors, i.e., HOA, COA, NOA, LO-OOA, MO-OOA, and LV-OOA, and (2) the mass spectra of OA factors are constant across the whole size ranges.

$$MS_{i,j} = \sum_{p=1}^{6} c_{i,j,p} \times ms_{OA,p} \qquad (3)$$

where MS$_{ij}$ is the mass spectrum of OA at size bin j and time-step i. ms$_{OA,p}$ is the normalized mass spectrum of OA factor p, and $c_{i,j,p}$ is the linear regression coefficients in dMdlogD_{va} (μg m^{-3}) which is constrained to be non-negative. The size distribution of each OA factor is finally normalized to the corresponding mass concentration of OA. In addition, only size-resolved mass spectra between 50–1200 nm were analyzed due to low signal-to-noise (S/N) ratio below 50 nm and above 1200 nm. The MS of NO$_3$-OA and SO$_4$-OA are not included in the analysis because the NO$_3$-OA factor contributes a very minor fraction of OA, while the OA in SO$_4$-OA shows overwhelmingly dominant *m/z* 28 and 44 peaks which might have a potential impact on linear regression coefficients. In addition, considering that SO$_4$-OA and NO$_3$-OA are mainly composed of sulfate and nitrate, respectively, similar size distributions of OA to sulfate and nitrate in these two factors are expected. Figure S7 shows a comparison of the size distributions of HOA and OOA derived from linear regression method and tracer-*m/z* method,

Title Page

Abstract | Introduction

Conclusions | References

Tables | Figures

|◄ | ►|

◄ | ►

Back | Close

Full Screen / Esc

Printer-friendly Version

Interactive Discussion

respectively (Zhang et al., 2005b). As the size distribution of OOA between the two methods is similar, HOA has some differences with generally higher concentrations below ∼ 150 nm for the tracer-*m/z* method.

3 Results and discussion

5 The mass spectral profiles of eight factors and the diurnal variations of OA in each factor are shown in Fig. 2. The chemical composition of each PMF factor and the distribution of PMF factors in each NR-species are shown in Fig. 3 and Table 1. In the following sections, we will describe each factor with a focus on mass spectra, diurnal variations, size distributions, and potential sources and processes.

10 ### 3.1 SO$_4$-OA and NO$_3$-OA

The SO$_4$-OA factor is primarily composed of ammonium sulfate, accounting for 82 % of the total mass of this factor (Fig. 3b). Not surprisingly, the SO$_4$-OA shows the best correlation ($r^2 = 0.97$) with sulfate followed by the oxygenated ion CO$_2^+$ (*m/z* 44, Fig. 4). Note that 18 % of OA is mixed within this factor and characterized by the highly oxidized 15 properties (O/C = 0.69). The OA in this factor is even more aged than the LV-OOA (O/C = 0.63) reported previously at the same location (Sun et al., 2011c). The diurnal profile of SO$_4$-OA is relatively flat (Fig. 5a) (Sun et al., 2011c). The results suggest that SO$_4$-OA is a highly aged secondary factor which is very likely from the regional transport. Indeed, sulfate in the SO$_4$-OA factor contributes 84 % of the total sulfate mass, 20 overall consistent with previous findings that ∼ 90 % of sulfate in NYC is from regional transport (Lall and Thurston, 2006; Qin et al., 2006). Comparatively, the sulfate in the rest of OA factors shows a pronounced noon peak, in agreement with the variation of gas-phase production rate of H$_2$SO$_4$. These results suggest the different sources of sulfate in SO$_4$-OA and other factors. In addition, the SO$_4$-OA factor does not contain 25 much nitrate likely due to (1) different formation mechanisms though they are both sec-

ondary products, and (2) ammonium nitrate is volatile, which is not favorable for the long-range transport.

The second factor (NO_3-OA) is dominantly contributed by ammonium nitrate (74 %) with the NO^+/NO_2^+ ratio (3.6) close to 3.5 determined from pure ammonium nitrate. The nitrate in NO_3-OA accounts for $\sim$ 80 % of total nitrate. The diurnal cycle of NO_3-OA shows high concentration in the early morning when temperature is low and the relative humidity is high (Fig. S8). The NO_3-OA concentration drops rapidly during daytime and shows the minimum in the late afternoon. Such diurnal variation is consistent with the diurnal profile of the equilibrium constant (K_p) of $NH_3(g) + HNO_3(g) \rightarrow NH_4NO_3(s)$, indicating that the partitioning between particle-phase nitrate and gas-phase HNO_3 might have played a major role (Sun et al., 2011c). The nitrate in the rest of OA factors presents a pronounced noon peak, consistent with the diurnal profile of gas-phase production of HNO_3 (Fig. 5b), which illustrates a dominant source of nitrate from photochemical production for these factors. The results above suggest that PMF analysis of the combined OA and IOA is able to reveal the two different formation mechanisms of nitrate. Note that this factor contains a majority of total chloride (45 %) that mainly exists in the form of NH_4Cl at AMS typical vaporizer temperatures (600 °C). The similar volatile characteristics of NH_4Cl to NH_4NO_3 further demonstrate the role of gas-to-particle partitioning in controlling this factor. The NO_3-OA factor mixes 17 % of fresh OA (O/C = 0.14), likely due to the condensation of fresh organic vapors on the nitrate particles, especially at nighttime. Although sulfate and nitrate are both secondary species and often internally mixed together, PMF analysis results clearly indicate their different formation and evolution processes since they are separated into different factors and appear not to mix each other.

3.2 HOA and COA

Similar to previously identified POA factors in NYC (Sun et al., 2011c), the HOA and COA show mass spectral profiles resembling to those from gas/diesel exhaust (Canagaratna et al., 2004) and cooking emissions (Mohr et al., 2009; Allan et al., 2010),

respectively. The HOA spectrum is characterized by the hydrocarbon ion series of $C_nH_{2n+1}^+$ and $C_nH_{2n-1}^+$, and very low O/C ratio (= 0.04), while the COA shows higher O/C ratio (= 0.13), and higher *m/z* 55/57 ratio (= 2.9) – a signature indicating the presence of COA (Mohr et al., 2012). The diurnal variations of HOA and COA are also
5 consistent with the emissions from traffic exhaust and cooking activities which are characterized by the distinct peaks corresponding to the specific times, e.g., traffic hours in the morning and meal times at noon and evening. While the HOA shows tight correlations with most of tracers for primary emissions, e.g., NO_x, B_{abs}, EC, etc., the COA shows the best correlation with some specific ions, e.g., $C_3H_3O^+$ and $C_6H_{10}O^+$ (Fig. 4).
10 HOA and COA together account for 23 % of total OA, which is slightly lower than 30 % previously reported in NYC (Sun et al., 2011c). Note that the two primary factors are almost completely organics (> 97 %) with little inorganic ammonium sulfate and ammonium nitrate. This is an evidence for the different sources between the primary organic particles and secondary inorganic species.
15   Figure 6 shows the diurnal evolution of the size distributions of six OA factors and Fig. 7 presents the average size distributions for the entire study. The diurnal cycle of HOA size distribution shows a bimodal distribution in both mid-night and morning rush hours when the small mode particles peaking at ∼ 110 nm are largely enhanced. Such feature is further illustrated by the average size distributions between 6:00–8:00 on 25
20 July when HOA dominated OA composition (35 %, Fig. 7c). The small particle mode gradually dissipates during daytime with the contribution of large mode correspondingly being increased. The average HOA size also shows a considerable fraction at accumulation mode, likely from the emissions of large HOA particles. The size distribution of COA, however, shows a broad accumulation mode (peaking at ∼ 300 nm) at
25 dinner time, such as the COA dominant (57 % of OA) period between 17:00–21:00 on 2 August. The HOA and COA together account for a major fraction of ultrafine mode particles (> 50 %) and show overall different size distributions from secondary species, consistent with the externally mixing characteristics of POA with secondary species.

3.3 NOA

The nitrogen-enriched OA (NOA), again, shows similar spectral pattern to that reported in Sun et al. (2011c), which is characterized by amine-related peaks, e.g., CH_4N^+ (m/z 30), $C_2H_4N^+$ (m/z 42), $C_3H_8N^+$ (m/z 58), and $C_4H_{10}N^+$ (m/z 72), etc. (McLafferty and Turecek, 1993) and high N/C ratio (0.08 in this study). Consistently, the NOA show tight correlations with these amine-related ions, e.g., $r^2 = 0.94$ for $C_3H_8N^+$. Our previous analysis showed that the NOA is likely from the amines emitted from industrial and/or marine plankton emissions that are oxidized and condensed on pre-existing particles via acid-base chemistry. A recent study by on-line measuring the atmospheric amines in Atlanta with an Ambient Pressure Proton Transfer Mass Spectrometer (AmPMS) observed high concentrations of trimethylamine and triethylamine at noon and in the afternoon when the photochemistry is the most intense during the day (Hanson et al., 2011). This is overall consistent with our observation of the pronounced NOA noon peak. Also note that the NH_3^+/NH_2^+ ratio of 0.92 is quite different from 1.26 from ammonium nitrate and ~ 1.2 in SO_4-OA and NO_3-OA (Table 2), which likely further indicate the presence of some N-containing compounds in addition to inorganic ammonium. Our new PMF analysis suggests that the NOA factor mixes a considerable amount of inorganic nitrate and sulfate (25 % together) from the photochemical production at noon. The particle acidity for the NOA factor by comparing the observed NH_4^+ ($NH_{4,measured}^+$) and that needed to fully neutralize SO_4^{2-}, NO_3^-, and Chl ($NH_{4,predict}^+ = 18 \times (2 \times SO_4^{2-}/96 + NO_3^-/62 + Chl/35.5)$) (Zhang et al., 2007b) shows a high deficit of NH_4^+ ($NH_{4,measured}^+/NH_{4,predict}^+ = 0.35$), indicating the acidic properties of the NOA factor. The acidic environment facilitates the conversion of gaseous and basic amines to particles followed by the subsequent condensation on pre-existing particles, consistent with the observations of broader size distributions of NOA (Figs. 6 and 7) (Sun et al., 2011c).

3.4 LO-OOA and MO-OOA

The previous SV-OOA is split into two factors, i.e., LO-OOA and MO-OOA, which shows distinct spectral patterns and diurnal profiles. The mass spectrum of LO-OOA is characterized by two prominent peaks, m/z 29 (mainly CHO^+) and 43 (mainly $C_2H_3O^+$), and shows much similarity to the SV-OOA component resolved from PMF analysis of thermally-denuded OA spectra during SOAR-1 (Docherty et al., 2011). Also, the low O/C ratio (= 0.27) and low fraction of m/z 44 (2.6 %) for LO-OOA are consistent with those of SV-OOA in Docherty et al. (2011). In addition, the LO-OOA show high fraction of $C_xH_yO_1^+$ family (40 %), most likely from carbonyl or alcohol function groups, while much lower contribution of $C_xH_yO_2^+$ family (5.3 %), mainly from carboxylic functional groups. The diurnal variation of LO-OOA shows some similarities to nitrate with higher concentration at night and lower concentration during daytime, indicating their similar volatile properties (Docherty et al., 2011). Note that a small noon peak in the diurnal profile of LO-OOA is also observed. The mass spectral features and diurnal variation of LO-OOA likely suggest that (1) LO-OOA is an intermediate aging product from freshly oxidized OA to highly oxidized OA (Docherty et al., 2011), and/or (2) LO-OOA might be driven by the partitioning of organic vapors between gas and particle phase, which is facilitated by the high humidity and low temperature.

The second OOA factor, i.e., MO-OOA, however, shows more oxidized properties with higher O/C ratio (= 0.48) and higher fraction of $C_xH_yO_2^+$ family (17 %). The mass spectrum of MO-OOA resembles to that of OOA factor widely observed at other sites (Ng et al., 2010), and also biogenic OA (Slowik et al., 2010a; Sun et al., 2011a) though it appears to show relatively lower m/z 43/44 ratio. Particularly, the spectrum of MO-OOA shows much similarity to a local SOA identified from PMF analysis of the unified dataset from AMS and PTR-MS measurements (Slowik et al., 2010b). The local SOA was found to be associated with local photochemical products of acetaldehyde and formaldehyde, indicating that MO-OOA also likely represents a local SOA. The diurnal cycle of MO-OOA presents a pronounced noon peak with the concentration starting

Title Page

Abstract | Introduction

Conclusions | References

Tables | Figures

|◄ | ►|

◄ | ►

Back | Close

Full Screen / Esc

Printer-friendly Version

Interactive Discussion

to increase at ~09:00 and peaking at 13:00. The subsequent decrease of MO-OOA after 13:00 is likely due to the further oxidation of MO-OOA to LV-OOA, consistent with the corresponding increase of LV-OOA. Figure 8a shows the time series of MO-OOA, HCHO and $O_x(= O_3 + NO_2)$. Overall, similar time trends were observed for these three species. The daily correlations between MO-OOA and HCHO, MO-OOA and O_x are significant during days with intense solar radiation, e.g., $r = 0.88$ and 0.90 for MO-OOA vs. HCHO on 22 and 24 July, respectively. Further, the diurnal cycle of MO-OOA is also very similar to that of HCHO as shown in Fig. 8b. Our previous analysis showed that ~70% of HCHO in NYC is from the photochemical production, ~44% of which is from the isoprene oxidation (Lin et al., 2012). All these results suggest that MO-OOA is a SOA product mainly from local photochemical processing, e.g., oxidation of biogenic VOCs. The diurnal size evolution of MO-OOA shows a much broader size distribution during the photochemical processing time, likely indicating the formation of smaller particles from photochemical production followed by condensation on pre-existing particles. Docherty et al. (2011) identified a medium-volatility OOA (MV-OOA) that comprises a higher-volatility MV-OOA (MV-OOA-hv) and a lower-volatility MV-OOA (MV-OOA-lv) during SOAR-1. The two MV-OOA factors correlate with O_x and WSOC significantly and show very similar diurnal cycles to that of MO-OOA in this study. Detailed analysis suggests that the photochemical processing is the major source of these two factors, consistent with our conclusions.

A re-look at the case study on 22 July (Sun et al., 2011b) also supports the photochemical production of MO-OOA with the processes co-varying with the solar radiation and the formation of HCHO (Fig. S9). The initial photochemical production in the early morning firstly leads to an increase of MO-OOA, and then followed by an increase of more aged LV-OOA after ~13:00. The formation of LV-OOA is coincidently corresponding to the decrease of MO-OOA, likely indicating an oxidation process from MO-OOA to LV-OOA. The regional transport from the south, however, appears to play more important roles in controlling the variation of highly aged OA in SO_4-OA factor, which shows a gradual increase from ~09:00 till 18:00, in agreement with the air masses from the

polluted regions to the south of NYC. Results here indicate that the OA evolution on 22 July is an aging process mixed with local photochemical production and regional transport.

We also note that the MO-OOA factor contains ∼ 20 % of inorganic species, but the fragment ion patterns are quite different from those of pure inorganic species (Table 2). For example, the ion ratio of NO^+/NO_2^+ in MO-OOA factor is 9.4, which is much higher than 3.5 of ammonium nitrate alone. High NO^+/NO_2^+ ratio is an indication for the presence of organic nitrates (Alfarra et al., 2006; Rollins et al., 2010) though the ratio may vary depending on the specific HR-AMS instruments (Farmer et al., 2010). Alfarra et al. (2006) reported a ratio of NO^+/NO_2^+ of 7.5 and 5.1 for the photooxidation of 1,3,5-TMB and α-pinene with NO_x, respectively. Similarly, high NO^+/NO_2^+ ratios were also observed for NO_3 oxidation of β-pinene (~ 10) (Fry et al., 2009), various monoterpene ($\sim$10–15) and isoprene (~ 5) (Bruns et al., 2010). These results together suggest that NO^+ and NO_2^+ in MO-OOA factor is likely from the contribution of organic nitrates, especially at noon time, which are formed via the photochemical oxidation of VOCs. The nitrate in MO-OOA factor contributes ∼ 12 % of total nitrate mass. If assuming that NO_x^+ fragments in MO-OOA are all from organic nitrates and on average account for ∼ 10 % of total organic nitrate signal, we estimate that organic nitrates in NYC contribute ∼ 7 % of total organics. In addition, the ratio of NH_3^+/NH_2^+ in MO-OOA factor is ∼ 0.9 which is lower than that of ammonium (∼ 1.2 in this study). This might also indicate the presence of nitrogenated organic compounds in addition to inorganic ammonium. We also observed SO^+ and SO_2^+ fragment ions, but very minor other sulfate-related ions, e.g., SO_3^+, HSO_3^+, and $H_2SO_4^+$ in MO-OOA. Unfortunately, we don't have evidence to conclude if these SO_x^+ ions are from organic sulfates or ammonium sulfate.

3.5 LV-OOA

The factor of LV-OOA shows very similar spectral pattern to previously reported LV-OOA (Ng et al., 2010; Sun et al., 2011c), which is characterized by high O/C ratio (= 0.59) and f_{44}(15 %). The diurnal profile of LV-OOA is distinct from other OA factors,

showing a gradual increase from noon till late afternoon despite the rising boundary layer. Note that the increase of LV-OOA appears to intrinsically correlate with the decrease LO-OOA and MO-OOA, likely indicating a photochemical oxidation progress from less oxidized OOA to highly oxidized LV-OOA. The size distribution of LV-OOA

5 presents a persistent and single large accumulation across the day. Although LV-OOA is highly aged, it does not mix much of ammonium sulfate and ammonium nitrate, further indicating the different sources of LV-OOA and highly aged OA in SO_4-OA. Indeed, the correlation between LV-OOA and sulfate from new PMF analysis is weaker than that from PMF analysis of OA only ($r^2 = 0.42$ vs. 0.66). It appears that the previous LV-OOA

10 (Sun et al., 2011c) comprises two highly aged OA factors primarily from regional (SO_4-OA) and local contributions (LV-OOA), respectively. Consistently, the contribution of the sum of highly oxidized SO_4-OA (12 %) and LV-OOA (19 %) to the total OA is close to that of LV-OOA ($\sim$ 30 %) reported previously (Sun et al., 2011c). Also, the combined size distribution of LV-OOA and SO_4-OA is very similar to that of sulfate (Fig. 7), which

15 is characterized by a large accumulation mode peaking at $\sim$ 600 nm. This further supports the similar aging properties and internally mixed characteristics for the highly aged OA and sulfate.

To further investigate the evolution of OA, the triangle plot (f44 vs. f43) (Ng et al., 2010) and the Van Krevelen diagram (Heald et al., 2010) are presented in Fig. 9. The

20 HOA, COA, NO_3-OA, and LO-OOA show similar low oxidative properties with varying f43, which are located at the bottom of the triangular region. As the progress of aging, OA evolves to the upper corner and shows more similar oxidative properties to MO-OOA and LV-OOA. However, the ensemble OA never reaches the high oxidation state of SO_4-OA. Since the triangle plot represents an integration of OOA factors, in which

25 m/z 44 and m/z 43 are primarily CO_2^+ and $C_2H_3O^+$, respectively. It is of interest to check the relationship between fCO_2^+ (fraction of CO_2^+ in OA) vs. $fC_2H_3O^+$ (fraction of $C_2H_3O^+$ in OA) (Fig. 9b). Clearly, different behaviors from f44 vs. f43 were observed. The POA factors of HOA and COA are located at the most left-bottom corner with the lowest fCO_2^+ and $fC_2H_3O^+$, LO-OOA and NO_3-OA, however, are still in the triangular

region with high fC$_2$H$_3$O$^+$ yet similar low fCO$_2^+$, indicating the different sources and properties from HOA and COA. It appears that the aging of OA is characterized by two pathways. The initial oxidization of fresh OA, e.g., HOA/COA appears to involve a synchronous increase of both fCO$_2^+$ and fC$_2$H$_3$O$^+$, and evolves into the triangular region first. The further oxidation of less oxidized OA, e.g., LO-OOA/NO$_3$-OA, however, appears to following a trend with a decrease of fC$_2$H$_3$O$^+$ and increase of fCO$_2^+$. The two evolving trends are consistent with the evolution of H/C vs. O/C in the Van Krevelen diagram. The initial oxidation of POA shows a steeper slope than -1, likely driven by the functionalization by incorporating carbonyl groups (Ng et al., 2011). The further oxidation of OA shows a shallower slope (~ -0.8), most likely from the additions of both acid and alcohol functional groups with little fragmentation (Ng et al., 2011) The evolution processes also lead to a change of the size distributions of OA factors (Fig. 7), and the size appears to progress from smaller to larger particles as a function of oxidization state.

4   Conclusions

PMF analysis was performed for the first time to the combined HR mass spectral matrices of OA and IOA from the HR-AMS measurements at QC in NYC in summer 2009. In this study, eight factors were identified, including a SO$_4$-OA that mixes primarily ammonium sulfate and highly oxidized OA from regional scale, a NO$_3$-OA that contains primarily ammonium nitrate, two POA factors, i.e., HOA and COA from traffic emissions and cooking activities, respectively, an amine-related NOA that mixes acidic ammonium sulfate and nitrate from local photochemical production, and three OOA factors, i.e., a LV-OOA likely from further oxidation of OOA, a more oxidized OOA (MO-OOA) and a less oxidized OOA (LO-OOA). Each OA factor shows distinct mass spectral profile and diurnal variation reflecting its unique sources and photochemical processes. The POA factors of HOA and COA contain minor ammonium sulfate and ammonium nitrate, elucidating the different sources and mixing characteristics between

POA and inorganic secondary species. In comparison to the previous PMF analysis in Sun et al. (2011c), a new MO-OOA factor representing a local photochemical product was identified. The diurnal profile of MO-OOA shows a pronounced noon peak and correlates well with HCHO and O_x. The much higher NO^+/NO_2^+ ratio in MO-OOA than ammonium nitrate alone demonstrates the potential formation of organic nitrates during the photochemical processing. The LO-OOA, however, appears to be mainly driven by the gas-to-particle partitioning or likely an intermediate oxidation product between POA and LV-OOA. The NOA factor shows a high deficit of cation, which facilitates the transformation of alkaline amines to aerosol particles in acidic environments. Further investigations of the evolution of OA factors suggest that the initial oxidation of POA and further oxidation of OOA appears to follow different mechanisms. The evolution of size distributions of OA factors is also distinct, but overall a progressing trend from smaller to larger particle mode as a function of oxidation state. Our results show that PMF analysis of the combined AMS HR matrices is of importance for improving our understanding on the sources, mixing characteristics, acidity, and evolution processes of atmospheric aerosols, thus, it is of great interest to perform the same analysis to other HR-AMS datasets.

Supplementary material related to this article is available online at: http://www.atmos-chem-phys-discuss.net/12/13299/2012/ acpd-12-13299-2012-supplement.pdf.

in this study, the New York State Department of Environmental Conservation for use of their facility, and the Queens College administration and staff for hosting this study.

References

Aiken, A. C., Salcedo, D., Cubison, M. J., Huffman, J. A., DeCarlo, P. F., Ulbrich, I. M., Docherty, K. S., Sueper, D., Kimmel, J. R., Worsnop, D. R., Trimborn, A., Northway, M., Stone, E. A., Schauer, J. J., Volkamer, R. M., Fortner, E., de Foy, B., Wang, J., Laskin, A., Shutthanandan, V., Zheng, J., Zhang, R., Gaffney, J., Marley, N. A., Paredes-Miranda, G., Arnott, W. P., Molina, L. T., Sosa, G., and Jimenez, J. L.: Mexico City aerosol analysis during MILAGRO using high resolution aerosol mass spectrometry at the urban supersite (T0) – Part 1: Fine particle composition and organic source apportionment, Atmos. Chem. Phys., 9, 6633–6653, doi:10.5194/acp-9-6633-2009, 2009.

Alfarra, M. R., Paulsen, D., Gysel, M., Garforth, A. A., Dommen, J., Prévôt, A. S. H., Worsnop, D. R., Baltensperger, U., and Coe, H.: A mass spectrometric study of secondary organic aerosols formed from the photooxidation of anthropogenic and biogenic precursors in a reaction chamber, Atmos. Chem. Phys., 6, 5279–5293, doi:10.5194/acp-6-5279-2006, 2006.

Allan, J. D., Williams, P. I., Morgan, W. T., Martin, C. L., Flynn, M. J., Lee, J., Nemitz, E., Phillips, G. J., Gallagher, M. W., and Coe, H.: Contributions from transport, solid fuel burning and cooking to primary organic aerosols in two UK cities, Atmos. Chem. Phys., 10, 647–668, doi:10.5194/acp-10-647-2010, 2010.

Bruns, E. A., Perraud, V. r., Zelenyuk, A., Ezell, M. J., Johnson, S. N., Yu, Y., Imre, D., Finlayson-Pitts, B. J., and Alexander, M. L.: Comparison of FTIR and particle mass spectrometry for the measurement of particulate organic nitrates, Environ. Sci. Technol., 44, 1056–1061, doi:10.1021/es9029864, 2010.

Canagaratna, M. R., Jayne, J. T., Ghertner, D. A., Herndon, S., Shi, Q., Jimenez, J. L., Silva, P. J., Williams, P., Lanni, T., Drewnick, F., Demerjian, K. L., Kolb, C. E., and Worsnop, D. R.: Chase studies of particulate emissions from in-use New York City vehicles, Aerosol Sci. Tech., 38, 555–573, 2004.

DeCarlo, P. F., Kimmel, J. R., Trimborn, A., Northway, M. J., Jayne, J. T., Aiken, A. C., Gonin, M., Fuhrer, K., Horvath, T., Docherty, K. S., Worsnop, D. R., and Jimenez, J. L.:

Title Page

Abstract	Introduction
Conclusions	References
Tables	Figures

|◄ | ►|

◄ | ►

Back | Close

Full Screen / Esc

Printer-friendly Version

Interactive Discussion

Field-deployable, high-resolution, time-of-flight aerosol mass spectrometer, Anal. Chem., 78, 8281–8289, 2006.

DeCarlo, P. F., Ulbrich, I. M., Crounse, J., de Foy, B., Dunlea, E. J., Aiken, A. C., Knapp, D., Weinheimer, A. J., Campos, T., Wennberg, P. O., and Jimenez, J. L.: Investigation of the sources and processing of organic aerosol over the Central Mexican Plateau from aircraft measurements during MILAGRO, Atmos. Chem. Phys., 10, 5257–5280, doi:10.5194/acp-10-5257-2010, 2010.

Docherty, K. S., Aiken, A. C., Huffman, J. A., Ulbrich, I. M., DeCarlo, P. F., Sueper, D., Worsnop, D. R., Snyder, D. C., Peltier, R. E., Weber, R. J., Grover, B. D., Eatough, D. J., Williams, B. J., Goldstein, A. H., Ziemann, P. J., and Jimenez, J. L.: The 2005 study of organic aerosols at riverside (SOAR-1): instrumental intercomparisons and fine particle composition, Atmos. Chem. Phys., 11, 12387–12420, doi:10.5194/acp-11-12387-2011, 2011.

Drewnick, F., Hings, S. S., DeCarlo, P. F., Jayne, J. T., Gonin, M., Fuhrer, K., Weimer, S., Jimenez, J. L., Demerjian, K. L., Borrmann, S., and Worsnop, D. R.: A new time-of-flight aerosol mass spectrometer (ToF-AMS) – instrument description and first field deployment., Aerosol Sci. Tech., 39, 637–658, 2005.

Dzepina, K., Volkamer, R. M., Madronich, S., Tulet, P., Ulbrich, I. M., Zhang, Q., Cappa, C. D., Ziemann, P. J., and Jimenez, J. L.: Evaluation of recently-proposed secondary organic aerosol models for a case study in Mexico City, Atmos. Chem. Phys., 9, 5681–5709, doi:10.5194/acp-9-5681-2009, 2009.

Farmer, D. K., Matsunaga, A., Docherty, K. S., Surratt, J. D., Seinfeld, J. H., Ziemann, P. J., and Jimenez, J. L.: Response of an aerosol mass spectrometer to organonitrates and organosulfates and implications for atmospheric chemistry, Proc. Natl. Acad. Sci. USA, 107, 6670-6675, doi:10.1073/pnas.0912340107, 2010.

Forster, P., Ramaswamy, V., Artaxo, P., Berntsen, T., Betts, R., Fahey, D. W., Haywood, J., Lean, J., Lowe, D. C., Myhre, G., Nganga, J., Prinn, R., Raga, G., Schulz, M., and Dorland, R. V.: Changes in atmospheric constituents and in radiative forcing, in: Climate Change 2007: The Physical Science Basis. Contribution of Working Group I to the Fourth Assessment Report of the Intergovernmental Panel on Climate Change, edited by: Solomon, S., Qin, D., Manning, M., Chen, Z., Marquis, M., Averyt, K. B., Tignor, M., and Miller, H. L., Cambridge University Press, Cambridge, UK and New York, NY, USA, 2007.

Fry, J. L., Kiendler-Scharr, A., Rollins, A. W., Wooldridge, P. J., Brown, S. S., Fuchs, H., Dubé, W., Mensah, A., dal Maso, M., Tillmann, R., Dorn, H.-P., Brauers, T., and Cohen, R. C.:

Organic nitrate and secondary organic aerosol yield from NO_3 oxidation of β-pinene evaluated using a gas-phase kinetics/aerosol partitioning model, Atmos. Chem. Phys., 9, 1431–1449, doi:10.5194/acp-9-1431-2009, 2009.

Hanson, D. R., McMurry, P. H., Jiang, J., Tanner, D., and Huey, L. G.: Ambient pressure proton transfer mass spectrometry: detection of amines and ammonia, Environ. Sci. Technol., 45, 8881–8888, doi:10.1021/es201819a, 2011.

Heald, C. L., Jacob, D. J., Park, R. J., Russell, L. M., Huebert, B. J., Seinfeld, J. H., Liao, H., and Weber, R. J.: A large organic aerosol source in the free troposphere missing from current models, Geophys. Res. Lett., 32, L18809, doi:10.1029/2005GL023831, 2005.

Heald, C. L., Kroll, J. H., Jimenez, J. L., Docherty, K. S., DeCarlo, P. F., Aiken, A. C., Chen, Q., Martin, S. T., Farmer, D. K., and Artaxo, P.: A simplified description of the evolution of organic aerosol composition in the atmosphere, Geophys. Res. Lett., 37, L08803, doi:10.1029/2010gl042737, 2010.

Heald, C. L., Coe, H., Jimenez, J. L., Weber, R. J., Bahreini, R., Middlebrook, A. M., Russell, L. M., Jolleys, M., Fu, T.-M., Allan, J. D., Bower, K. N., Capes, G., Crosier, J., Morgan, W. T., Robinson, N. H., Williams, P. I., Cubison, M. J., DeCarlo, P. F., and Dunlea, E. J.: Exploring the vertical profile of atmospheric organic aerosol: comparing 17 aircraft field campaigns with a global model, Atmos. Chem. Phys., 11, 12673–12696, doi:10.5194/acp-11-12673-2011, 2011.

Jayne, J. T., Leard, D. C., Zhang, X., Davidovits, P., Smith, K. A., Kolb, C. E., and Worsnop, D. R.: Development of an aerosol mass spectrometer for size and composition analysis of submicron particles, Aerosol Sci. Tech., 33, 49–70, 2000.

Jimenez, J. L., Canagaratna, M. R., Donahue, N. M., Prevot, A. S. H., Zhang, Q., Kroll, J. H., DeCarlo, P. F., Allan, J. D., Coe, H., Ng, N. L., Aiken, A. C., Docherty, K. S., Ulbrich, I. M., Grieshop, A. P., Robinson, A. L., Duplissy, J., Smith, J. D., Wilson, K. R., Lanz, V. A., Hueglin, C., Sun, Y. L., Tian, J., Laaksonen, A., Raatikainen, T., Rautiainen, J., Vaattovaara, P., Ehn, M., Kulmala, M., Tomlinson, J. M., Collins, D. R., Cubison, M. J., E, Dunlea, J., Huffman, J. A., Onasch, T. B., Alfarra, M. R., Williams, P. I., Bower, K., Kondo, Y., Schneider, J., Drewnick, F., Borrmann, S., Weimer, S., Demerjian, K., Salcedo, D., Cottrell, L., Griffin, R., Takami, A., Miyoshi, T., Hatakeyama, S., Shimono, A., Sun, J. Y., Zhang, Y. M., Dzepina, K., Kimmel, J. R., Sueper, D., Jayne, J. T., Herndon, S. C., Trimborn, A. M., Williams, L. R., Wood, E. C., Middlebrook, A. M., Kolb, C. E., Baltensperger, U., and Worsnop, D. R.: Evolution of organic aerosols in the atmosphere, Science, 326, 1525–1529, doi:10.1126/science.1180353, 2009.

Factor analysis of combined organic and inorganic aerosol spectra

Y. L. Sun et al.

Title Page

Abstract | Introduction

Conclusions | References

Tables | Figures

◄ | ►|

◄ | ►

Back | Close

Full Screen / Esc

Printer-friendly Version

Interactive Discussion

Khan, B., Hays, M. D., Geron, C., and Jetter, J.: Differences in the OC/EC ratios that charac-
terize ambient and source aerosols due to thermal-optical analysis, Aerosol Sci. Tech., 46,
127–137, doi:10.1080/02786826.2011.609194, 2011.

Lall, R. and Thurston, G. D.: Identifying and quantifying transported vs. local sources of New
York City $PM_{2.5}$ fine particulate matter air pollution, Atmos. Environ., 40, 333–346, 2006.

Lanz, V. A., Alfarra, M. R., Baltensperger, U., Buchmann, B., Hueglin, C., and Prévôt, A. S. H.:
Source apportionment of submicron organic aerosols at an urban site by factor analytical
modelling of aerosol mass spectra, Atmos. Chem. Phys., 7, 1503–1522, doi:10.5194/acp-7-
1503-2007, 2007.

Lin, Y. C., Schwab, J. J., Demerjian, K. L., Bae, M.-S., Chen, W.-N., Sun, Y., Zhang, Q.,
Hung, H.-M., and Perry, J.: Summertime formaldehyde observations in new york city: am-
bient levels, sources and its contribution to HO_x radicals, J. Geophys. Res., 117, D08305,
doi:10.1029/2011JD016504, 2012.

McLafferty, F. W. and Turecek, F.: Interpretation of Mass Spectra, University Science Books,
Mill Valley, California, 1993.

Mohr, C., Huffman, J. A., Cubison, M. J., Aiken, A. C., Docherty, K. S., Kimmel, J. R., Ul-
brich, I. M., Hannigan, M., and Jimenez, J. L.: Characterization of primary organic aerosol
emissions from meat cooking, trash burning, and motor vehicles with high-resolution aerosol
mass spectrometry and comparison with ambient and chamber observations, Environ. Sci.
Technol., 43, 2443–2449, doi:10.1021/es8011518, 2009.

Mohr, C., DeCarlo, P. F., Heringa, M. F., Chirico, R., Slowik, J. G., Richter, R., Reche, C.,
Alastuey, A., Querol, X., Seco, R., Peñuelas, J., Jiménez, J. L., Crippa, M., Zimmermann, R.,
Baltensperger, U., and Prévôt, A. S. H.: Identification and quantification of organic aerosol
from cooking and other sources in Barcelona using aerosol mass spectrometer data, Atmos.
Chem. Phys., 12, 1649–1665, doi:10.5194/acp-12-1649-2012, 2012.

Ng, N. L., Canagaratna, M. R., Zhang, Q., Jimenez, J. L., Tian, J., Ulbrich, I. M., Kroll, J. H.,
Docherty, K. S., Chhabra, P. S., Bahreini, R., Murphy, S. M., Seinfeld, J. H., Hildebrandt, L.,
Donahue, N. M., DeCarlo, P. F., Lanz, V. A., Prévôt, A. S. H., Dinar, E., Rudich, Y., and
Worsnop, D. R.: Organic aerosol components observed in Northern Hemispheric datasets
from Aerosol Mass Spectrometry, Atmos. Chem. Phys., 10, 4625–4641, doi:10.5194/acp-10-
4625-2010, 2010.

Ng, N. L., Canagaratna, M. R., Jimenez, J. L., Chhabra, P. S., Seinfeld, J. H., and Worsnop, D. R.: Changes in organic aerosol composition with aging inferred from aerosol mass spectra, Atmos. Chem. Phys., 11, 6465–6474, doi:10.5194/acp-11-6465-2011, 2011.

Paatero, P. and Tapper, U.: Positive matrix factorization: a non-negative factor model with optimal utilization of error estimates of data values, Environmetrics, 5, 111–126, 1994.

Pope III, C. A., Burnett, R. T., Thun, M. J., Calle, E. E., Krewski, D., Ito, K., and Thurston, G. D.: Lung cancer, cardiopulmonary mortality, and long-term exposure to fine particulate air pollution, JAMA- J. Am. Med. Assoc., 287, 1132–1141, 2002.

Pope III, C. A., Ezzati, M., and Dockery, D. W.: Fine-particulate air pollution and life expectancy in the United States, N. Engl. J. Med., 360, 376–386, doi:10.1056/NEJMsa0805646, 2009.

Qin, Y., Kim, E., and Hopke, P. K.: The concentrations and sources of $PM_{2.5}$ in metropolitan New York City, Atmos. Environ., 40, 312–332, 2006.

Rollins, A. W., Fry, J. L., Hunter, J. F., Kroll, J. H., Worsnop, D. R., Singaram, S. W., and Cohen, R. C.: Elemental analysis of aerosol organic nitrates with electron ionization high-resolution mass spectrometry, Atmos. Meas. Tech., 3, 301–310, doi:10.5194/amt-3-301-2010, 2010.

Schauer, J. J. and Cass, G. R.: Source apportionment of wintertime gas-phase and particle-phase air pollutants using organic compounds as tracers, Environ. Sci. Technol., 34, 1821–1832, 2000.

Slowik, J. G., Stroud, C., Bottenheim, J. W., Brickell, P. C., Chang, R. Y.-W., Liggio, J., Makar, P. A., Martin, R. V., Moran, M. D., Shantz, N. C., Sjostedt, S. J., van Donkelaar, A., Vlasenko, A., Wiebe, H. A., Xia, A. G., Zhang, J., Leaitch, W. R., and Abbatt, J. P. D.: Characterization of a large biogenic secondary organic aerosol event from eastern Canadian forests, Atmos. Chem. Phys., 10, 2825–2845, doi:10.5194/acp-10-2825-2010, 2010a.

Slowik, J. G., Vlasenko, A., McGuire, M., Evans, G. J., and Abbatt, J. P. D.: Simultaneous factor analysis of organic particle and gas mass spectra: AMS and PTR-MS measurements at an urban site, Atmos. Chem. Phys., 10, 1969–1988, doi:10.5194/acp-10-1969-2010, 2010b.

Sun, Y., Zhang, Q., Zheng, M., Ding, X., Edgerton, E. S., and Wang, X.: Characterization and source apportionment of water-soluble organic matter in atmospheric fine particles ($PM_{2.5}$) with high-resolution aerosol mass spectrometry and GC–MS, Environ. Sci. Technol., 45, 4854–4861, doi:10.1021/es200162h, 2011a.

Discussion Paper | Discussion Paper | Discussion Paper | Discussion Paper

Title Page

Abstract | Introduction

Conclusions | References

Tables | Figures

◄◄ | ►►

◄ | ►

Back | Close

Full Screen / Esc

Printer-friendly Version

Interactive Discussion

Sun, Y. L., Zhang, Q., Schwab, J. J., Chen, W. N., Bae, M. S., Lin, Y. C., Hung, H. M., and Demerjian, K. L.: A case study of aerosol processing and evolution in summer in New York City, Atmos. Chem. Phys., 11, 12737–12750, doi:10.5194/acp-11-12737-2011, 2011b.

Sun, Y.-L., Zhang, Q., Schwab, J. J., Demerjian, K. L., Chen, W.-N., Bae, M.-S., Hung, H.-M., Hogrefe, O., Frank, B., Rattigan, O. V., and Lin, Y.-C.: Characterization of the sources and processes of organic and inorganic aerosols in New York City with a high-resolution time-of-flight aerosol mass spectrometer, Atmos. Chem. Phys., 11, 1581–1602, doi:10.5194/acp-11-1581-2011, 2011c.

Turpin, B. J. and Huntzicker, J. J.: Identification of secondary organic aerosol episodes and quantitation of primary and secondary organic aerosol concentrations during SCAQS, Atmos. Environ., 29, 3527–3544, 1995.

Ulbrich, I. M., Canagaratna, M. R., Zhang, Q., Worsnop, D. R., and Jimenez, J. L.: Interpretation of organic components from Positive Matrix Factorization of aerosol mass spectrometric data, Atmos. Chem. Phys., 9, 2891–2918, doi:10.5194/acp-9-2891-2009, 2009.

Ulbrich, I. M., Canagaratna, M. R., Cubison, M. J., Zhang, Q., Ng, N. L., Aiken, A. C., and Jimenez, J. L.: Three-dimensional factorization of size-resolved organic aerosol mass spectra from Mexico City, Atmos. Meas. Tech., 5, 195–224, doi:10.5194/amt-5-195-2012, 2012.

Volkamer, R., Jimenez, J. L., Martini, F. S., Dzepina, K., Zhang, Q., Salcedo, D., Molina, L. T., Molina, M. J., and Worsnop, D. R.: Secondary organic aerosol formation from anthropogenic VOCs: rapid and higher than expected, Geophys. Res. Lett., 33, L17811, doi:10.1029/2006GL026899, 2006.

Watson, J. G.: Visibility: science and regulation, J. Air Waste Manage. Assoc., 52, 628–713, 2002.

Wood, E. C., Canagaratna, M. R., Herndon, S. C., Onasch, T. B., Kolb, C. E., Worsnop, D. R., Kroll, J. H., Knighton, W. B., Seila, R., Zavala, M., Molina, L. T., DeCarlo, P. F., Jimenez, J. L., Weinheimer, A. J., Knapp, D. J., Jobson, B. T., Stutz, J., Kuster, W. C., and Williams, E. J.: Investigation of the correlation between odd oxygen and secondary organic aerosol in Mexico City and Houston, Atmos. Chem. Phys., 10, 8947–8968, doi:10.5194/acp-10-8947-2010, 2010.

Zhang, Q., Alfarra, M. R., Worsnop, D. R., Allan, J. D., Coe, H., Canagaratna, M. R., and Jimenez, J. L.: Deconvolution and quantification of hydrocarbon-like and oxygenated organic aerosols based on aerosol mass spectrometry, Environ. Sci. Technol., 39, 4938–4952, doi:10.1021/es048568l, 2005a.

Title Page

Abstract | Introduction

Conclusions | References

Tables | Figures

◄◄ | ►►

◄ | ►

Back | Close

Full Screen / Esc

Printer-friendly Version

Interactive Discussion

Zhang, Q., Worsnop, D. R., Canagaratna, M. R., and Jimenez, J. L.: Hydrocarbon-like and oxygenated organic aerosols in Pittsburgh: insights into sources and processes of organic aerosols, Atmos. Chem. Phys., 5, 3289–3311, doi:10.5194/acp-5-3289-2005, 2005b.

Zhang, Q., Jimenez, J. L., Canagaratna, M. R., Allan, J. D., Coe, H., Ulbrich, I., Alfarra, M. R., Takami, A., Middlebrook, A. M., Sun, Y. L., Dzepina, K., Dunlea, E., Docherty, K., De-Carlo, P. F., Salcedo, D., Onasch, T., Jayne, J. T., Miyoshi, T., Shimono, A., Hatakeyama, S., Takegawa, N., Kondo, Y., Schneider, J., Drewnick, F., Weimer, S., Demerjian, K., Williams, P., Bower, K., Bahreini, R., Cottrell, L., R.J.Griffin, Rautiainen, J., Sun, J. Y., Zhang, Y. M., and Worsnop, D. R.: Ubiquity and dominance of oxygenated species in organic aerosols in anthropogenically-influenced Northern Hemisphere mid-latitudes, Geophys. Res. Lett., 34, L13801, doi:10.1029/2007GL029979, 2007a.

Zhang, Q., Jimenez, J. L., Worsnop, D. R., and Canagaratna, M.: A case study of urban particle acidity and its effect on secondary organic aerosol, Environ. Sci. Technol., 41, 3213–3219, 2007b.

Zhang, Q., Jimenez, J. L., Canagaratna, M. R., Allan, J. D., Coe, H., Ulbrich, I., Alfarra, M. R., Takami, A., Middlebrook, A. M., Sun, Y. L., Dzepina, K., Dunlea, E., Docherty, K., DeCarlo, P. F., Salcedo, D., Onasch, T., Jayne, J. T., Miyoshi, T., Shimono, A., Hatakeyama, S., Takegawa, N., Kondo, Y., Schneider, J., Drewnick, F., Weimer, S., Demerjian, K., Williams, P., Bower, K., Bahreini, R., Cottrell, L., R.J.Griffin, Rautiainen, J., Sun, J. Y., Zhang, Y. M., and Worsnop, D. R.: Understanding atmospheric organic aerosols via factor analysis of aerosol mass spectrometry: a review, Anal. Bioanal. Chem., 401, 3045–3067, doi:10.1007/s00216-011-5355-y, 2011.

Zheng, M., Cass, G. R., Schauer, J. J., and Edgerton, E. S.: Source apportionment of $PM_{2.5}$ in the Southeastern United States using solvent-extractable organic compounds as tracers, Environ. Sci. Technol., 36, 2361–2371, 2002.

Factor analysis of combined organic and inorganic aerosol spectra

Y. L. Sun et al.

Table 1. Summary of mass concentrations ($\mu g\,m^{-3}$) of NR species in PMF factors.

PMF Factor	Org	SO_4	NO_3	NH_4	Chl
SO_4-OA	0.785	2.665	0.003	0.920	0.004
NO_3-OA	0.118	0.060	0.387	0.140	0.011
HOA	0.818	0.011	0.005	0.004	0.003
COA	0.741	0.015	0.004	0.002	0.000
NOA	0.194	0.036	0.021	0.007	0.000
LO-OOA	1.175	0.086	0.008	0.003	0.005
MO-OOA	1.576	0.254	0.061	0.067	0.000
LV-OOA	1.278	0.030	0.001	0.054	0.001

Table 2. Summary of the fraction (%) of selected fragment ions, and ion ratios in eight PMF factors. The average ion ratios for the entire study, and NO^+/NO_2^+ and NH_3^+/NH_2^+ from ammonium nitrate are also shown.

Factor	NO^+	NO_2^+	NO^+/NO_2^+	NH_2^+	NH_3^+	NH_3^+/NH_2^+	SO^+	SO_2^+	SO_3^+	SO_2^+/SO^+	SO_3^+/SO^+
SO_4-OA	0.08			13.1	15.7	1.20	16.1	19.6	3.29	1.22	0.20
NO_3-OA	43.6	12.0	3.6	9.20	11.0	1.20	1.79	2.08	0.23	1.16	0.13
HOA	0.55			0.21	0.26	1.27	0.20	0.27		1.33	
COA	0.50			0.21	0.01	0.04	0.40	0.60		1.50	
NOA	6.81	1.56	4.4	1.42	1.31	0.92	3.19	4.03	0.54	1.26	0.17
LO-OOA	0.63					0.22	1.14	1.42	0.71	1.25	0.62
MO-OOA	2.87	0.31	9.4	1.83	1.66	0.91	2.97	4.08		1.37	
LV-OOA	0.09			1.70	2.17	1.28	0.16				
Entire study			3.8			1.19				1.22	0.19
NH_4NO_3			3.5			1.26					

Title Page

Abstract | Introduction

Conclusions | References

Tables | Figures

◀◀ | ▶▶

◀ | ▶

Back | Close

Full Screen / Esc

Printer-friendly Version

Interactive Discussion
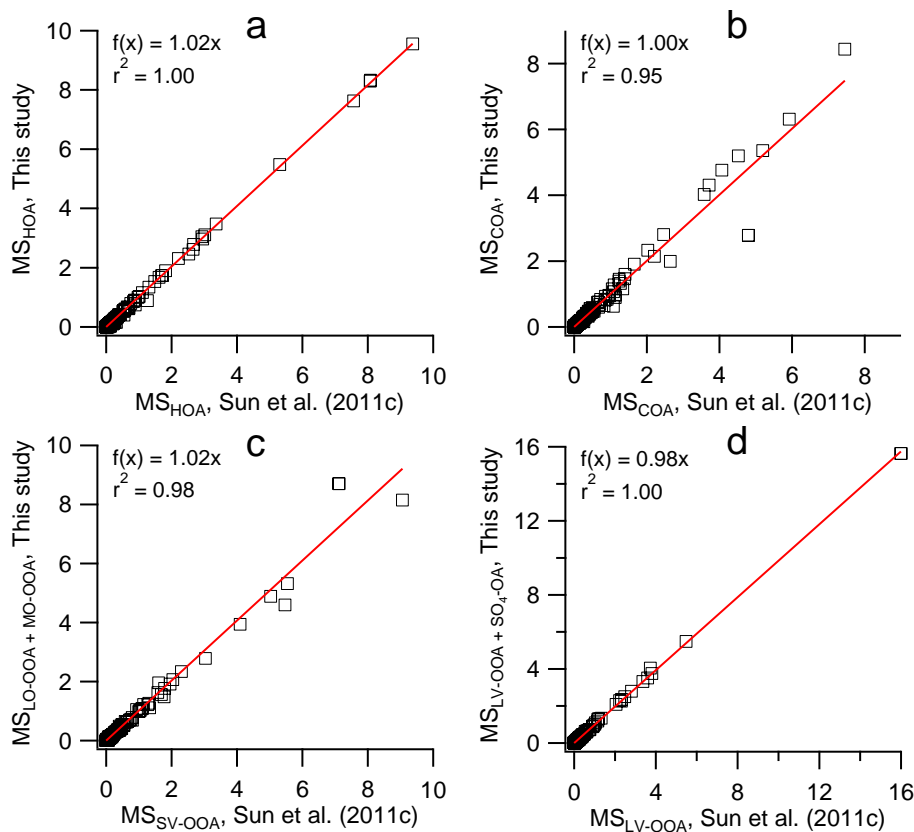
Fig. 1. Mass spectra (MS) comparison of **(a)** HOA, **(b)** COA, **(c)** LO-OOA + MO-OOA vs. SV-OOA, and **(d)** LV-OOA + SO_4-OA vs. LV-OOA from 8-factor solution of PMF analysis of the combined organic and inorganic aerosols in this study and 5-factor solution of PMF analysis of OA in Sun et al. (2011c).

Discussion Paper | Discussion Paper | Discussion Paper | Discussion Paper |

Title Page

Abstract | Introduction

Conclusions | References

Tables | Figures

|◄ | ►|

◄ | ►

Back | Close

Full Screen / Esc

Printer-friendly Version

Interactive Discussion
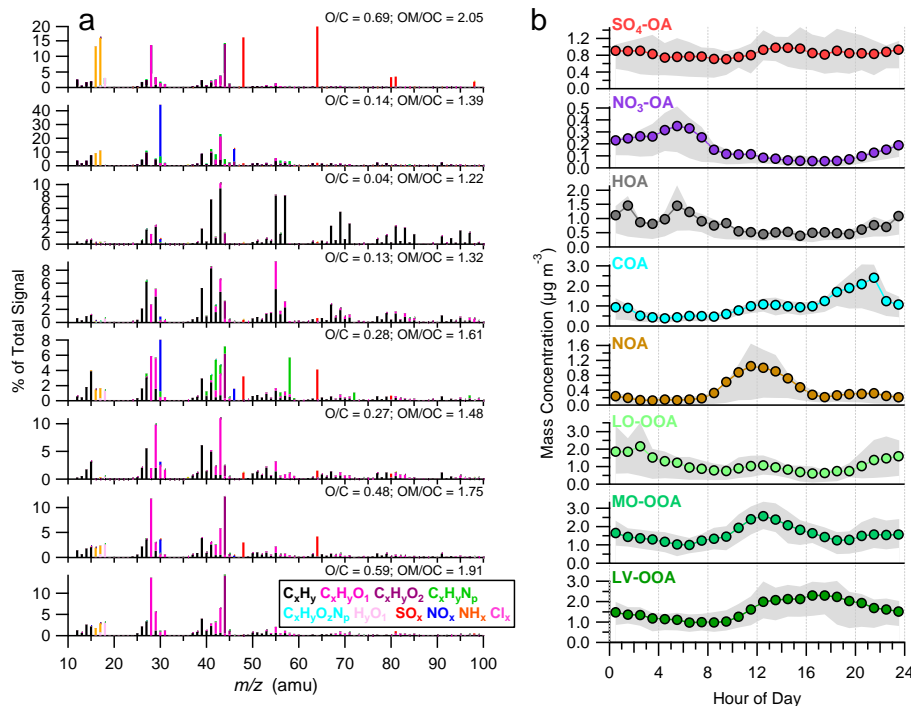
Fig. 2. (a) High resolution mass spectra of PMF factors. The mass spectra of OA in SO$_4$-OA and NO$_3$-OA are enhanced by a factor of 3 and 10, respectively, for clarity. **(b)** Diurnal profiles of OA in each factor. The solid circles refer to mean values, and the gray shaded areas are 25th and 75th percentiles.

Title Page

Abstract | Introduction

Conclusions | References

Tables | Figures

|◀ | ▶|

◀ | ▶

Back | Close

Full Screen / Esc

Printer-friendly Version

Interactive Discussion
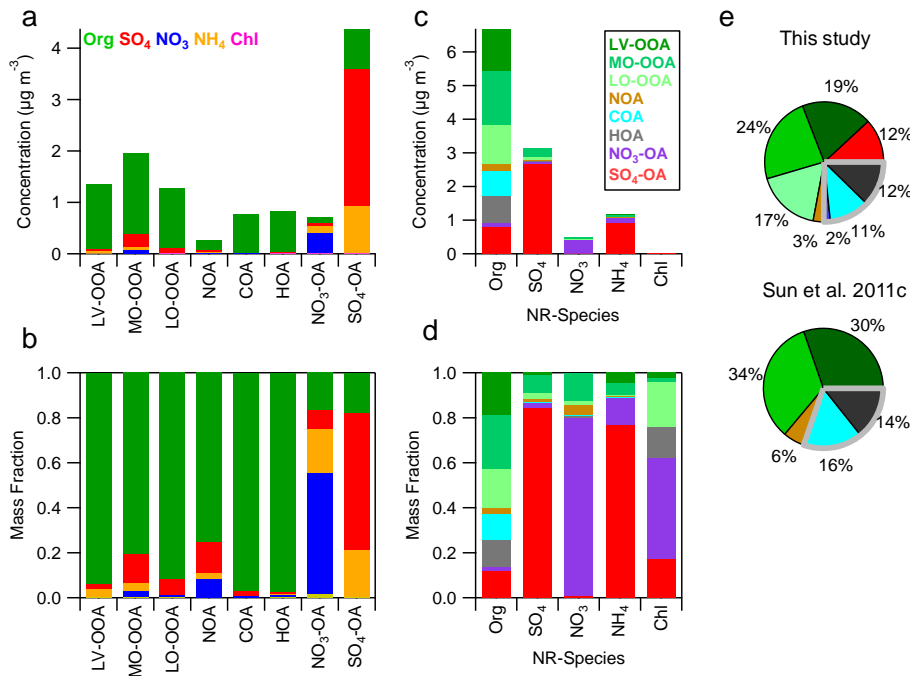
Fig. 3. (a, b) Chemical composition of PMF factors, i.e., mass concentrations and mass fractions of NR-species (organics, sulfate, nitrate, ammonium, and chloride) in each factor; **(c, d)** Distribution of PMF factors in each NR-species; **(e)** Average composition of OA in this study and 5-factor OA (LV-OOA, SV-OOA, HOA, COA, and NOA) composition in Sun et al. (2011c).
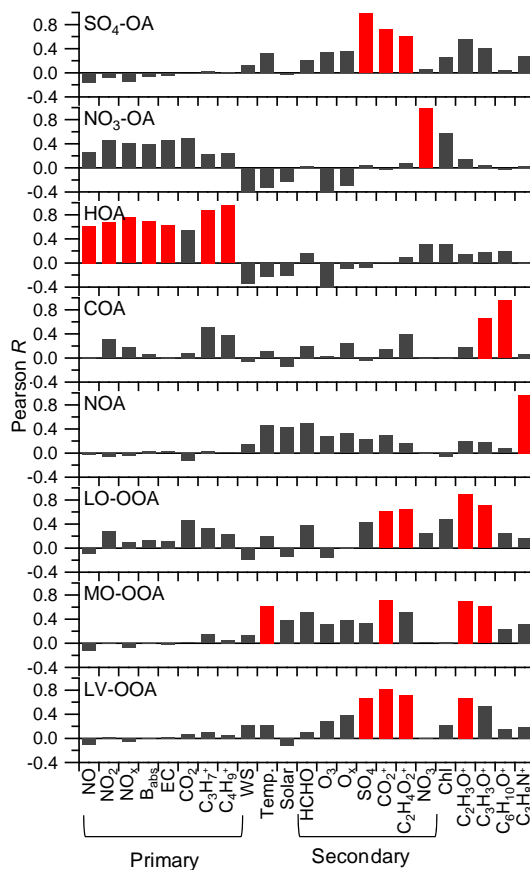
Fig. 4. Correlation coefficients of PMF factors versus external tracers. The correlation coefficients with the values larger than 0.6 are marked as red.

Title Page

Abstract | Introduction

Conclusions | References

Tables | Figures

◄ | ►I

◄ | ►

Back | Close

Full Screen / Esc

Printer-friendly Version

Interactive Discussion
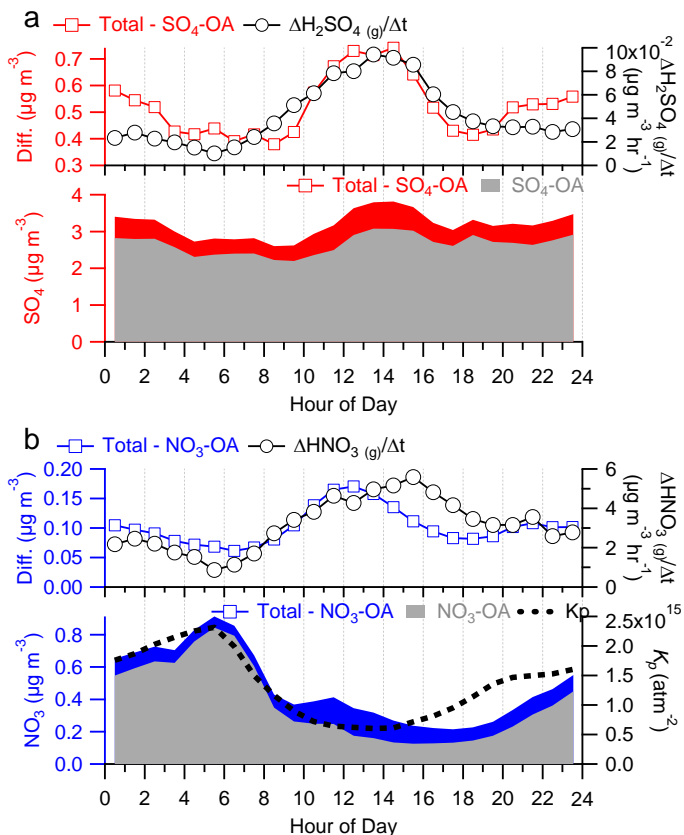
Fig. 5. Diurnal cycles of **(a)** sulfate in SO_4-OA and the rest of OA factors, and the estimated gas-phase production rate of H_2SO_4 (Sun et al., 2011c), **(b)** nitrate in NO_3-OA and the rest of OA factors, the estimated gas-phase production rate of HNO_3, and equilibrium constant of K_p (Sun et al., 2011c).
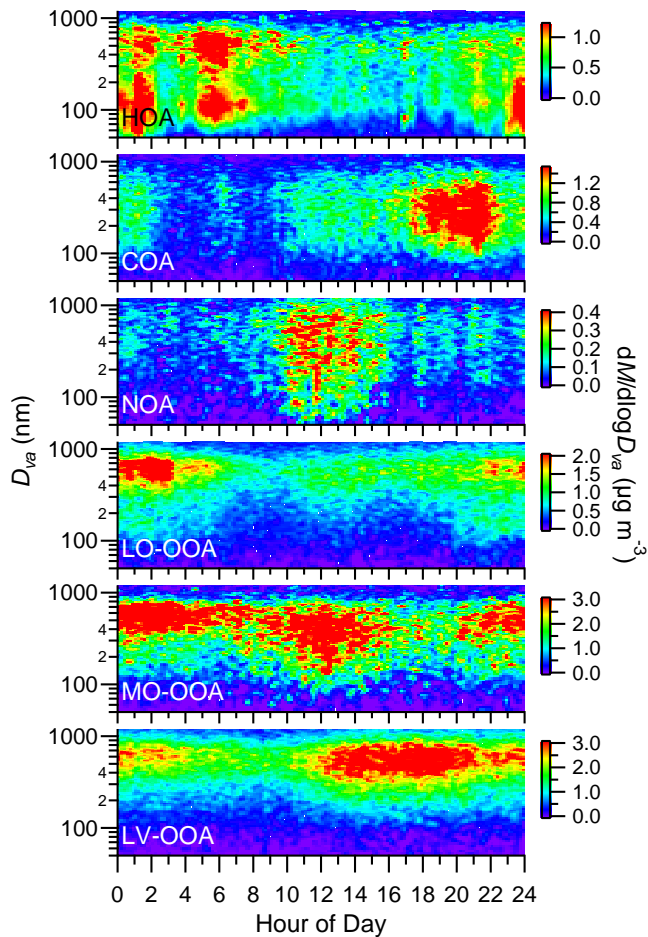
Fig. 6. Diurnal evolution of size distributions of six OA factors from linear regression method. Note all the size distributions were smoothed by 3 points using binominal algorithm.

Title Page

Abstract | Introduction

Conclusions | References

Tables | Figures

|◄ | ►|

◄ | ►

Back | Close

Full Screen / Esc
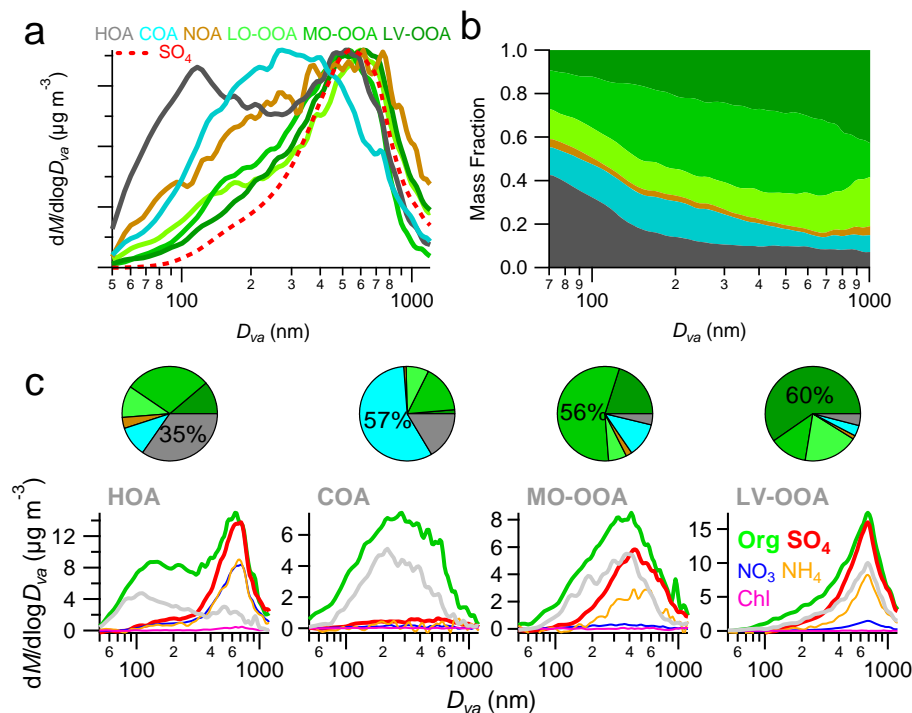
Fig. 7. (a) Average size distributions of six OA factors and sulfate (dash line) for the entire study. Each size distribution is scaled to the maximum. **(b)** The mass fraction of OA factors as a function of size. **(c)** shows the average size distributions of NR-PM$_1$ species for selected periods with OA being dominated by HOA (6:00–8:00, 25 July), COA (17:00–21:00, 2 August), MO-OOA (10:00–14:00, 18 July), and LV-OOA (18:00, 17 July–4:00, 18 July), respectively. The size distributions of dominant OA factors are shown as gray lines. The pie charts show the average OA composition for each selected time period.

13333

a

b
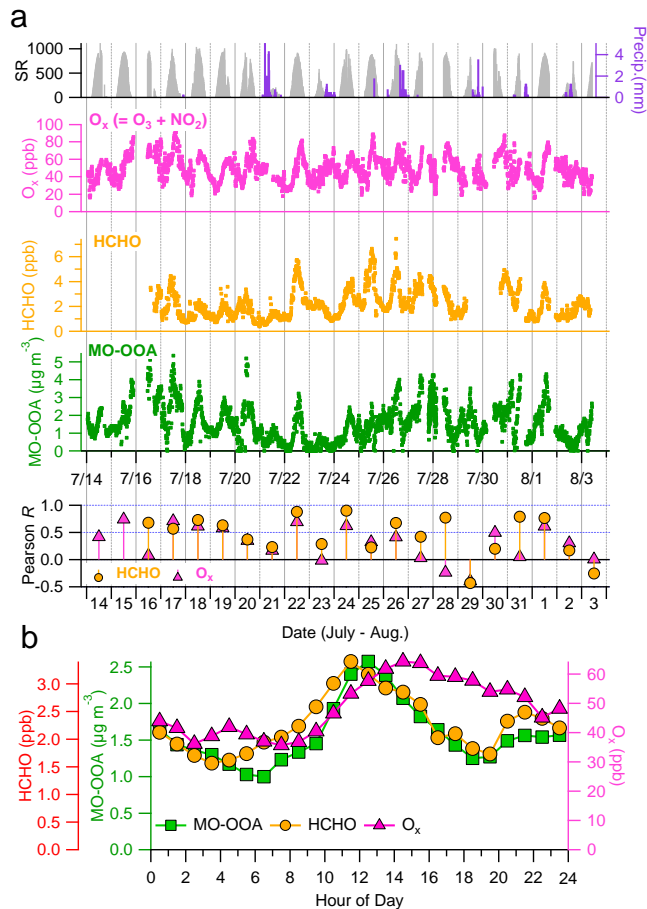
Fig. 8. (a) Time series of solar radiation (SR) and precipitation, $O_x (= NO_2 + O_3)$, HCHO, and MO-OOA, and daily correlations of MO-OOA vs. HCHO, and MO-OOA vs. O_x. **(b)** Diurnal profiles of MO-OOA, HCHO, and O_x for the entire study.

Title Page

Abstract | Introduction

Conclusions | References

Tables | Figures

|◄ | ►|

◄ | ►

Back | Close

Full Screen / Esc

Printer-friendly Version

Interactive Discussion
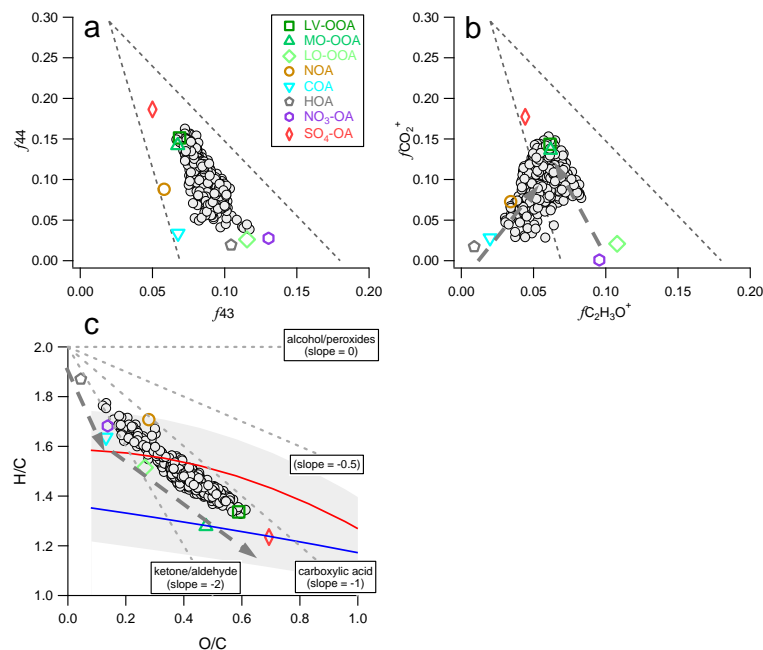
Fig. 9. (a, b) Hourly averaged $f44$ (fraction of m/z 44 in OA) vs. $f43$ (fraction of m/z 43 in OA), and fCO_2^+ (fraction of CO_2^+ in OA) vs. $fC_2H_3O^+$ (fraction of $C_2H_3O^+$ in OA). The $f44$ vs. $f43$ and fCO_2^+ vs. $fC_2H_3O^+$ relationships for eight OA factors are also shown. The dash lines in **(a)** and **(b)** refer to a triangular region that encompasses ambient OOA factors determined from PMF analyses of 43 AMS datasets (Ng et al., 2010). **(c)** Van Krevelen diagram for hourly averaged OA and eight OA factors. The dash lines indicate the changes of H/C against O/C due to adding specific functional groups to an aliphatic carbon (Heald et al., 2010). The red and blue lines are derived from the right and left lines in the triangle plot, and the light gray shaded region denotes ±10% uncertainty (Ng et al., 2011).